---

**Article:**
Alanazi, N. and Susmel, L. orcid.org/0000-0001-7753-9176 (2022) Theory of critical distances and static/dynamic fracture behaviour of un-reinforced concrete: length scale parameters vs. material meso-structural features. Engineering Fracture Mechanics, 261. 108220. ISSN 0013-7944

https://doi.org/10.1016/j.engfracmech.2021.108220

---

# Theory of Critical Distances and static/dynamic fracture behaviour of un-reinforced concrete: length scale parameters vs. material meso-structural features

*N. Alanazi* [a,b] *and L. Susmel* [a]

[a]Department of Civil and Structural Engineering, The University of Sheffield, Mappin Street, Sheffield, S1 3JD, United Kingdom
[b]Department of Civil Engineering, College of Engineering, University of Hail, Hail, 81411, Kingdom of Saudi Arabia

**Corresponding Author:** Prof. Luca Susmel
Department of Civil and Structural Engineering
The University of Sheffield, Mappin Street, Sheffield, S1 3JD, UK
Telephone: +44 (0) 114 222 5073
E-mail: l.susmel@sheffield.ac.uk

## Abstract

The Theory of Critical Distances (TCD) groups together a number of approaches that make use of specific length scale parameters to model and estimate the strength of cracked/notched engineering materials. In the TCD framework, the critical distance is assumed to be an intrinsic property and this length is somehow related to the material micro-/meso-/macro-structural features. In recent years, a number of comprehensive theoretical/experimental investigations proved that the TCD is successful also in assessing the static/dynamic Mode I/Mixed-Mode I-II strength of unreinforced concrete containing geometrical features of all kinds. However, the scientific community has not yet agreed on a commonly accepted answer to the most obvious fundamental research question, i.e. *"what is the physical meaning of the TCD critical distance?"* In order to answer this question, a number of experimental results were generated by testing specimens of unreinforced concrete under static and dynamic Mode I bending. According to what is recommended by RILEM for the determination of fracture parameters of plain concrete, this comprehensive experimental work involved not only plain samples, but also specimens containing crack-like saw-cut notches. The specimens being tested were manufactured by using different bespoke mixes so that the meso-structural features of the concrete materials being tested could be controlled and then modelled in a very accurate way. The results from this systematic experimental/theoretical study led to the conclusion that, as far as the specific unreinforced concrete mixes used in the present investigation are concerned, the TCD critical length approaches the average distance between the crack-like saw-cut notch tip line and the first aggregates, with these aggregates acting as barriers slowing down/affecting the crack propagation process.

**Keywords:** Concrete; Notch; Theory of Critical Distances; length scale parameters; fracture process zone.

**Nomenclature**

| | |
|---|---|
| 3PB | three-point bending |
| $a_f$, $b_f$ | Material constant to calibrate $\sigma_f$ vs. $\dot{Z}$ relationship. |
| $a_k$, $b_k$ | Material constant to calibrate $K_{Id}$ vs. $\dot{Z}$ relationship. |
| $a_L$, $b_L$ | Material constant to calibrate L vs. $\dot{Z}$ relationship. |
| FPZ | fracture process zone |
| $d_{agg}$ | aggregate size |
| $d_s$ | average inter-aggregate distance |
| $d_m$ | distance from the notch tip to the nearest aggregate particle at the mid-thickness |
| $d_c$ | average distance from the notch tip to the nearest aggregate barrier |
| $L_{ch}$ | Hillerborg's characteristic length |
| $L_{FPZ}$ | length of the fracture process zone |
| L | TCD critical distance under quasi-static loading |
| $\ell$ | length scale parameter determined according to Gradient Elasticity |
| $L_D$ | TCD critical distance under dynamic loading |
| $\sigma_f$ | tensile strength |
| $K_c$ | fracture toughness |
| $K_{Ic}$ | plain strain fracture toughness |
| $K_{Id}$ | dynamic fracture toughness |
| θ, r | polar coordinates |
| $K_{t,b}$ | stress concentration factor under bending |
| $r_n$ | notch root radius |
| $\sigma_{nom}$ | nominal stress |
| $\sigma_{eff}$ | effective stress |
| $\sigma_y$ | Mode I stress perpendicular to the notch bisector |
| $\sigma_{UTS}$ | ultimate tensile strength |
| $\sigma_f$ | tensile strength |
| $\sigma_{fn}$ | strength of notched concrete with respect to net area. |
| $\dot{Z}$ | reference dynamic variable |
| $\dot{\Delta}_c$ | displacement rate |
| $A_i$ | area of region of interest |
| $W_i$ | width of region of interest. |
| $d_i$ | average distance associated with a region of interest |

# 1 Introduction

Concrete is a heterogeneous material whose meso-structure is based on three key elements, i.e., cement paste, aggregates, and the transition regions at the interface between the two. As far as its mechanical response is concerned, concrete exhibits a quasi-brittle behaviour [1]. In this context, very often the level of non-linearity characterising concrete's stress-strain curves is so little that, for the sake of simplicity, its behaviour is modelled by adopting a simple linear-elastic constitutive law.

Turning to unreinforced concrete beams containing pre-existing defects/flaws, their final breakage under both static and dynamic loading is preceded by the formation of a sizable Fracture Process Zone (FPZ) ahead of the traction-free cracks [1]. The material surrounding the FPZ is seen to always deform in a way which is predominately elastic [2–4]. In this setting, the FPZ represents the portion of material that controls the overall strength of the concrete under investigation. As the magnitude of the local stresses increases, the number of micro-cracks that initiate and propagate within the FPZ increases, with these micro-cracks occupying almost the entire process zone when the material reaches the incipient failure condition [3].

The available state-of-the-art knowledge makes it evident that, over the years, the international scientific community has made a tremendous effort to observe and understand those physical processes leading to the initiation and propagation of the micro-cracks in the FPZ. These comprehensive studies involved the use of different experimental techniques such as, for instance, electron microscope [5–8], x-ray based techniques [9,10], acoustic emission [11–14], and ultrasonic measurements [15].

By tackling this problem from different angles, the international scientific community has worked systematically also to quantify the size of the FPZ. As to this aspect, a number of studies [16–18] available in the technical literature seem to converge to the common idea that the characteristic length, $L_{FPZ}$, defining the size of the FPZ in concrete is somehow linked with the maximum aggregate size, $d_{agg}$. For instance, Bažant [19] states that $L_{FPZ}$ is a multiple of $d_{agg}$ that ranges in the interval $d_{agg}$-$12 \cdot d_{agg}$.

The available technical literature shows also that the size of the FPZ has been attempted to be quantified using different theoretical frameworks such as, for instance, the Fictitious Crack Model [20] and the Crack Band Method [21]. In this setting, Hillerborg et al. [20] took full advantage of the Fictitious Crack Model to derive a simple expression suitable for determining a material characteristic length, $L_{ch}$, that links the static strength, $\sigma_f$, with the critical stress intensity factor, $K_c$, i.e.:

$$L_{ch} = \left(\frac{K_c}{\sigma_f}\right)^2 \tag{1}$$

In this setting, characteristic length $L_{ch}$ is treated a material intrinsic property [22]. In concrete, $L_{FPZ}$ is proportional to $L_{ch}$ [3,23,24] and varies in the range $0.3L_{ch}$-$0.5L_{ch}$ [24]. Similarly, based on a sophisticated reasoning, Karihaloo [25] argued that $L_{FPZ}$ can directly be estimated from $L_{ch}$ as follows:

$$L_{FPZ} = \frac{1}{\pi} L_{ch} = \frac{1}{\pi}\left(\frac{K_c}{\sigma_f}\right)^2 \tag{2}$$

Turning to the problem of designing unreinforced concrete containing geometrical features of all kinds, the Theory of Critical Distances (TCD) has proven to be a promising method, with its usage resulting in accurate results both under static and dynamic loading [26,27]. The TCD groups together a number of design methods that post-process the linear-elastic stress fields in the vicinity of the stress raisers being assessed by making use of a specific material length scale parameter [23]. In the TCD framework, the critical distance is treated as a material property that is different for different materials. Further, the TCD characteristic length is related to the micro-, meso-, or macro-structural features of the material under investigation as well as to the characteristics of the cracking behaviour being displayed [23, 28]. As far as brittle/quasi-brittle materials are concerned, the TCD length scale parameter, L, is estimated under static loading according to the following well-known definition [29–31]:

$$L = \frac{1}{\pi}\left(\frac{K_{Ic}}{\sigma_f}\right)^2 \tag{3}$$

where $\sigma_f$ is, again, the material tensile strength and $K_{Ic}$ is the plane strain fracture toughness. As far as concrete is concerned, the TCD length scale parameter is seen to be of order of a few millimetres [23,26,32]. Further, according to Shah et al. [24] as well as to Karihaloo [25] – see also Eq. (2), definition (3) suggests that the TCD length scale parameter, L, is directly related to the size of the FPZ.

The same key ingredients on which the TCD is based can also be used to design notched concrete by taking full advantage of Gradient Elasticity (GE) [33]. GE is a very sophisticated theory that makes use of constitutive laws which are enriched through specific material length scale parameters [34]. Similar to the TCD, the GE length scale parameter, $\ell$, is related to the micro-/meso-/macro-structural features of the material being assessed [35]. This results in the fact that GE length parameter $\ell$ can directly be estimated from the TCD critical distance as follows [35]:

$$\ell \approx \frac{L}{2\sqrt{2}} = \frac{1}{2\sqrt{2}} \times \frac{1}{\pi}\left(\frac{K_{Ic}}{\sigma_f}\right)^2 \tag{4}$$

Eqs. (2), (3) and (4) suggest that GE critical length $\ell$ as well is somehow related to the size of the FPZ.

Given the complex and challenging scenario briefly discussed above, the ultimate goal of the research work summarised in the present paper is to find possible links between the TCD critical distance, the length of the FPZ, and concrete's meso-structural features. This will be done by considering not only quasi-static, but also dynamic situations. To this end, a series of static/dynamic bending tests were conducted on specimens containing crack-like saw-cut notches [36] that were manufactured by using different concrete mixes.

## 2 The TCD assessment of static/dynamic Mode I loading

Examination of the state of art shows that the cracking behaviour and the mechanical properties of concrete under dynamic loading are different from those observed under quasi-static loading [37,38]. In particular, it is well-known that the strength of concrete increases as the loading rate (and, consequently, the strain rate) increases. As to this aspect, it is reported that the dynamic strength of unreinforced concrete can be up to six times larger than the corresponding static strength [37]. In this context, it is worth observing that a number of analytical expressions have been proposed in the technical literature [39,40] to model and estimate the dynamic strength of concrete as a function of the applied strain rate. As to the above approaches, it is interesting to observe that, although some of them are very complex, ultimately they are all based on power laws [26].

As done for the strength, a limited number of experimental studies were carried out to investigate also the effect of the loading/strain rate on the fracture toughness of concrete [41,42]. These studies all confirmed that the fracture toughness of concrete increases as the loading/strain rate increases. Further, the change in the response of the fracture toughness with the applied strain rate is seen to follow a linear trend in a log-log schematisation. This suggests that, in unreinforced concrete, also the link between the dynamic fracture toughness, $K_{Id}$, and the load/strain rate can be model by adopting simple power laws [26].

If $\dot{Z}$ is used to denote either the loading rate, the stress rate, the displacement rate, the strain rate, or the stress intensity factor rate, according to the considerations reported above, the strength and the fracture toughness of un-reinforced concrete can then be expressed via simple power laws as follows [26,27]:

$$\sigma_f(\dot{Z}) = a_f(\dot{Z})^{b_f} \tag{5}$$

$$K_{Id}(\dot{Z}) = a_K(\dot{Z})^{b_K} \tag{6}$$

Eq. (5) and Eq. (6) can be used to extend definition (3) to the dynamic case, so that a suitable expression for the TCD critical distance can be written directly as follows:

$$L(\dot{Z}) = \frac{1}{\pi}\left[\frac{K_{Id}(\dot{Z})}{\sigma_f(\dot{Z})}\right]^2 = a_L(\dot{Z})^{b_L} \quad (7)$$

In power laws (5) to (7), material constants $a_f$, $b_f$, $a_K$, $b_K$, $a_L$, and $b_L$ can be either calibrated experimentally or derived theoretically [26,27].

The TCD groups together a number of design methods [23] that all make use of a suitable critical distance – Eq. (7) – to calculate an effective design stress, $\sigma_{eff}(\dot{Z})$. This effective design stress is then used to estimate directly the extent of damage associated with the linear elastic stress field acting on the process zone. The simplest formalisation of the TCD is usually referred to as the Point Method (PM) [23]. According to Peterson's intuition [43], the PM postulates that the effective stress has to be taken equal to the linear-elastic stress determined at a distance from the assumed crack initiation point equal to $L(\dot{Z})/2$ [23]. As suggested by Neuber [44,45], the TCD can be formalised also in terms of the Line Method (LM). According to the LM, the effective stress is calculated by averaging the local linear-elastic stress over a line having length equal to $2L(\dot{Z})$ [23]. These two formalisations of the TCD are the simplest ones to be used in situations of practical interest. However, it is worth mentioning here that there are more sophisticated ways to calculate $\sigma_{eff}(\dot{Z})$, namely the Area Method (AM) and the Volume Method (VM) [46,47]. According to the AM, $\sigma_{eff}(\dot{Z})$ is determined by averaging the local stress over a semi-circular area centred at the notch/crack tip and having radius equal to $1.32 \cdot L(\dot{Z})$ [48]. In contrast, according to the VM, $\sigma_{eff}(\dot{Z})$ is calculated by averaging the local linear-elastic stresses over a hemispherical volume centred at the notch/crack tip and having radius equal to $1.54 \cdot L(\dot{Z})$ [48].

Having briefly defined the general features of the different formalisations of the TCD, the discussion reported in what follows will focus on the use of this theory to assess the strength of notched unreinforced concrete subjected to static/dynamic Mode I loading.

The use of the TCD as a design tool takes as its starting point the idea that notched concrete will fail as soon as the effective stress estimated according to either the PM, LM, AM, or VM becomes equal to the plain material strength, i.e. [26]:

$$\text{when } \sigma_{eff}(\dot{Z}) = \sigma_f(\dot{Z}) \Rightarrow \text{failure} \tag{8}$$

If attention is focused solely on the simplest formalisations of the TCD, the PM and LM can be expressed mathematically as follows [26,27]:

$$\boldsymbol{\sigma_{eff}(\dot{Z}) = \sigma_y\left(\theta = 0, r = \frac{L(\dot{Z})}{2}\right)} \quad \text{(PM)} \tag{9}$$

$$\boldsymbol{\sigma_{eff}(\dot{Z}) = \frac{1}{2L(\dot{Z})}\int_0^{2L(\dot{Z})} \sigma_y(\theta = 0, r)\,dr} \quad \text{(LM)} \tag{10}$$

where the meaning of the adopted symbols as well as the orientation of the system of coordinates being used are defined and explained in Fig. 1.

According to Eq. (7), the length scale parameter needed to estimate the effective stress through Eqs. (9) and (10) depends on both $K_{Id}(\dot{Z})$ and $\sigma_f(\dot{Z})$. However, since concrete in the TCD framework can be treated as a quasi-brittle material, when $K_{Id}(\dot{Z})$ is not available, there is an alternative procedure to estimate $L(\dot{Z})$ [26]. In more detail, under a specific value of $\dot{Z}$, the use of this simplified methodology to determine $L(\dot{Z})$ is based on two sets of results generated by testing (i) a series of un-notched specimens and (ii) a series of specimens containing a known geometrical feature (preferably a notch which as sharp as possible [28,49]). The plain specimens are used to quantify $\sigma_f(\dot{Z})$. The results from the calibration notched specimens are used instead to post-process the linear-elastic stress fields in the vicinity of the tips of the tested notches. In this context, the relevant stress fields can be estimated either numerically or analytically. Given then the linear-elastic stress distribution along the notch bisector in the incipient failure condition, according to Fig. 2, the point at which the straight horizontal line

corresponding to $\sigma_f(\dot{Z})$ and the above stress-distance curve intersect with each other allows the value of $L(\dot{Z})/2$ to be determined unambiguously. Clearly, in order to calibrate constants $a_L$ and $b_L$ in power law (7), the procedure sketched in Fig. 2 should be used to estimate $L(\dot{Z})$ under at least two different values of $\dot{Z}$.

In what follows, this simplified procedure will be used to determine $L(\dot{Z})$ for the different concrete mixes being considered in the present investigation.

## 3 Experimental details and numerical stress analysis

Un-notched and notched concrete specimens were fabricated by adopting different concrete mix designs. These specimens were tested under static/dynamic bending and all the experimental results were generated in the Structures Laboratory of the University of Sheffield, UK.

As summarised in Tab. 1, a total of four mix proportions were employed in this study. All specimens were manufactured by mixing Portland Cement having strength class equal to 32.5 MPa with grade M sand. The water-to-cement ratio (w/c) was set equal to 0.44 and superplasticizer Sika® ViscoFlow® 2000 was added to enhance concrete workability and prevent the segregation of the aggregates. The mixes being tested were prepared by using two different single-size coarse aggregates (Fig. 3), with this being done to obtain material morphologies with specific, controlled mesoscopic features. Concrete mixes with Low-Coarse (LC) aggregates and Dense-Coarse (DC) aggregates were prepared with 10.5 mm single-size aggregates, whereas concrete mixes with relatively Low-Fine (LF) aggregates and Dense-Fine (DF) aggregates were prepared using 5.5 mm single-size aggregates. Both 10.5 mm and 5.5 mm aggregates were extracted by sieving well-distributed natural rounded river gravel with a nominal size of 10 mm. The 10.5 mm aggregates were taken out by using a sieve with opening equal to 12.5 mm and then collected by using a sieve with opening equal to 9.5 mm. In contrast, the 5.5 mm aggregates were extracted by trapping them between two sieves having opening equal to 6.3 mm and 4.75 mm, respectively.

Further, for any value of the aggregate size, $d_{agg}$, being considered, the average inter-aggregate distance, $d_s$, was changed by changing the content (i.e., the percentage) of the single-size gravel. Separation $d_s$ was determined as the average from the distances between adjacent aggregates that were measured in two specimens randomly selected from any concrete mix being investigated. Any specimen used to quantify $d_s$ was cut along two planes perpendicular to the longitudinal axis. Subsequently, the digital high-resolution pictures of the obtained cross-sections were post-processed by using a standard image processing software. Fig. 4 shows some examples of the cut cross-sections obtained from the four mixes. According to this simple procedure, $d_s$ was measured to be equal to 4.8 mm, 2.8 mm, 3.3 mm, and 1.9 mm in the LC, DC, LF, and DF concrete mix, respectively (see also Tab. 4). As mentioned above, these separation values were determined from the two cross sections of two specimens randomly selected from any concrete mix being manufactured. While these values give a representative indication of the average inter-aggregate distance for the various mixes that were investigated, certainly an accurate quantification of separation $d_s$ would have required the use of a larger number of individual measurements. However, given the large intrinsic variability associated with the mesostructure of concrete, the $d_s$ values measured according to this simple procedure were considered to be enough accurate and representative to allow the post-processing of the generated experimental data to be performed in a reliable way.

Turning back to the specimens' fabrication process, the fresh concrete prepared by using the mixes described above was cast into steel moulds, sealed in plastic sheets, and then kept at room temperature. The specimens were de-moulded after twenty-four hours and then stored in a controlled-environment room until the day of testing.

As per the technical drawings reported in Fig. 5, the square section specimens had nominal gross cross-sectional area equal to 75 mm × 75 mm and length equal to 285 mm. Both notched and un-notched prisms had a net width equal to 50 mm to eliminate any possible size effect on the results being generated. All the experimental tests were run under three-point bending (3PB), with the span between the lower supports being equal to 225 mm. The sharp U-notches

having notch root radius, $r_n$, equal to 1.3 mm were fabricated using a circular tip blade having thickness equal to 2.6 mm.

The tests were performed using a hydraulic actuator with a loading cell attached to the bottom of the piston rod to ensure that the peak force was measured accurately not only under static, but also under dynamic loading. A digital unit was used to control the displacement of the actuator as well as the overall testing procedure. A pre-load of about 0.2 kN was applied to ensure that the specimens were in full contact with the loading rollers before testing. The ramp loads were applied by controlling the traveling speed of the actuator.

A high-speed camera synchronised with the signals gathered both from the loading cell and from the actuator's LVDT was employed to measure the displacements via Digital Image Correlation (DIC). Using this full-field, non-contact optical technique, the vertical displacement vs. time curves were determined by post-processing the videos being recorded. This was done by targeting the slit tip in the notched specimens and the bottom of the mid-span gauge length in the plain specimens. For any experimental result being generated, the displacement rate was calculated from the slope of the corresponding vertical DIC displacement vs. time curve. The results generated by testing both the notched and the plain specimens were obtained by making the displacement rates vary in the range 0.007-3.91 mm/s.

All the experimental results that were generated are summarized in Tables 2 and 3 for the plain and notched specimens, respectively. For the sake of clarity, the same results are plotted also in Fig. 6 as a function of the vertical displacement rate, $\dot{\Delta}_c$. Figs 6a to 6d show the experimental results of the un-notched specimens presented in terms of concrete static/dynamic strength, $\sigma_f(\dot{Z})$, which is calculated, in the incipient failure condition, according to the beam theory. In a similar way, Figs 6e to 6h summarise the experimental results generated by testing the notched specimens in terms of nominal-net stress, $\sigma_{fn}(\dot{Z})$, at the notch tip section.

Fig. 7 shows the fracture surfaces observed in eight different notched specimens made using different concrete mixes and tested under different displacement rates.

The static properties for every concrete mix being considered were determined by averaging the results generated by testing the un-notched specimens under quasi-static bending. According to this simple procedure, the flexural strength was determined to be equal to 5.3 MPa for the LC mix, to 4.8 MPa for the DC mix, to 5.3 MPa for the LF mix, and, finally, to 3.9 MPa for the DF mix. As to these values, it can be highlighted that $\sigma_f(\dot{\Delta}_c)$ was seen to decrease as the aggregate content increased. A possible explanation is that those processes resulting in the final breakage of concrete are preceded by the formation of micro-cracks, with these micro-cracks being more likely to initiate at the interface between aggregates and cement paste [50]. This is due to the fact that these regions are prone to contain pre-existing micro-cracks and pores that facilitate/favour the fracturing process by acting as localised stress concentrators [50,51]. Therefore, since the extension of the aggregate/cement interface area increases as the aggregate content increases, the presence of larger amounts of gravel was seen to lower the overall strength of the concrete mixes being tested.

Having described in detail the experimental procedure that was used to implement the present study, it is important to highlight that the cracking behaviour of concrete materials is markedly affected by important manufacturing variables such as, for instance, type of aggregate, aggregate size, water-to-cement ratio, and curing process. Accordingly, care should be taken when the results from the present theoretical/experimental work are attempted to be extended to concrete materials manufactured using different mixes and different manufacturing protocols.

Finally, turning to the numerical stress analyses, the relevant stress fields in the notched specimens (Fig. 5b) were determined by modelling the concrete under investigation as a homogenous and isotropic material [26,52]. The linear-elastic stress fields in the vicinity of the assessed notches were determined numerically via commercial Finite Element (FE) software ANSYS®. The specimens were modelled using 4-node structural plane elements, with the mesh in the vicinity of the notch tip being refined gradually until convergence occurred. This standard numerical procedure returned a stress concentration factor under bending, $K_{t,b}$, equal to 4.83.

## 4 Possible physical interpretations of TCD length scale parameter L

The TCD is a design methodology that combines Linear Elastic Fracture Mechanics (LEFM) with continuum mechanics to derive a specific critical length scale parameter – see Eqs (3) and (7). In this setting, the TCD critical distance can be thought of as a physical property which depends on the characteristics of the fracture processes, the micro-/meso-/macro-structural features and the intrinsic toughening mechanisms characterising the material being assessed [22, 27].

The TCD makes its predictions by directly post-processing the linear-elastic stress fields in the vicinity of the crack/notch tips. The different formalisations of the TCD can be derived by simply changing size and shape of the integration domain used to calculate the effective design stress. In this setting, independently of the specific form of the TCD being considered, the size of the integration domain is seen to be always proportional to L or $L(\dot{Z})$.

Since the beginning of 2000s, the TCD has been widely employed to design real structural components not only because it is easy-to-use and accurate, but also because it can be applied by directly post-processing the results from standard FE simulations solved using commercial FE codes. In these situations of practical interest, the required critical distance is derived either by adopting standard theoretical definitions – such as, for instance, Eq. (3) for the static case - or by adopting alternative experimental procedures like the one summarised in Fig. 2 and discussed in Ref. [53].

However, despite this success at an industrial level, examination of the state of the art suggests that the international scientific community has not yet agreed on a univocal interpretation of the physical meaning of the TCD critical distance. Thus, establishing an explicit link between the underlying material micro-/meso-/macro-structure and the associated critical distance is a fundamental challenge that is still under investigation, with the problem being tackled from different theoretical/experimental angles.

Focusing on the application of the TCD on unreinforced concrete, in a number of related studies [23,26,32] it was seen that the TCD critical length is of the order of a few millimetres.

This seems to suggest that this critical distance is somehow related to the features of the concrete morphology at a mesoscopic level.

Jadallah et al. [32] experimentally investigated the accuracy of the TCD in estimating the fatigue limit of notched unreinforced concrete beams. To this end, they used a large number of experimental results generated by testing U-notched specimens under four-point bending. These specimens were manufactured by changing the water-to-cement ratio, while the proportions of the other mix ingredients were kept constant. This comprehensive experimental campaign proved that the TCD can be employed successfully also to estimate the fatigue limit of notched concrete. With regard to this experimental/theoretical work, it is important to highlight that a high level of accuracy was obtained by taking the critical distance invariably equal to 5.8 mm. According to the way the specimens were manufactured, the geometrical features of the material at a mesoscopic level (i.e., aggregate size and average inter-aggregate distance) were the same in the two different batches being tested. In contrast, the change in the water-to-cement ratio resulted in a change in the concrete mechanical strength. Since, as mentioned above, accurate estimates were obtained by taking the critical distance constant and equal to 5.8 mm, it is reasonable to believe that, as far as fatigue of unreinforced concrete is concerned, the TCD length scale parameter is linked to the material meso-structural features and not to the strength.

By testing U-notched beams under four-point bending, Pelekis and Susmel [26] investigated experimentally the accuracy of the TCD in assessing the strength of unreinforced concrete also when it is subjected to static and dynamic Mode I loading. They found that accurate predictions could be made by taking the TCD critical distance equal to 4.8 mm, with this holding true independently of the value of the applied displacement rate. In this setting, it is important to point out that this value for the TCD critical distance was seen to approach the average inter-aggregate distance that was estimated to be of the order of 5 mm.

The outcomes from the experimental/theoretical investigations briefly discussed above seem to converge the idea that, as far as un-reinforce concrete is concerned, the TCD length scale parameter is somehow linked with the geometrical characteristics of the dominant source of

inherent meso-structural heterogeneity [23,54]. Since the aggregate content represents about 60% to 70% of the total concrete volume [55], according to the above reasoning, one may argue that the critical distance should be linked either to the aggregates size, $d_{agg}$, or to the average inter-aggregate distance, $d_s$ – i.e., the average distance between adjacent aggregates.

As discussed in Section 3, in the present investigation, the specimens being tested were manufactured by considering two aggregate sizes, i.e., either $d_{agg}$=10.5 mm or $d_{agg}$=5.5 mm. Further, the mixes were prepared so that it was possible to test specimens having average inter-aggregate distance, $d_s$, ranging from 1.9 mm up to 4.75 mm (see Tab. 4).

In order to find possible links between the TCD length scale parameter and the meso-structural features of the concrete being tested, the critical distance was calculated for every mix design under investigation by following the simplified procedure described in Section 2 and summarised in Fig. 2. In particular, initially the results generated by testing the un-notched specimens were used to calibrate the power laws – Eq. (5) - needed to quantify and model the static/dynamic strength of the concrete mixes being investigated. Constants $a_f$ and $b_f$ in Eq. (5) were calibrated using the standard least-squares method as shown by the trend straight-lines seen in Fig. 6a to 6d. According to this simple procedure, the following relationships for each mix design were derived as a function of the vertical displacement rate, $\dot{\Delta}_c$:

$$\text{Mix LC} \Rightarrow \sigma_f(\dot{\Delta}_c) = 6.00 \cdot \dot{\Delta}_c^{0.030} \ \text{[MPa]} \tag{11}$$

$$\text{Mix DC} \Rightarrow \sigma_f(\dot{\Delta}_c) = 5.61 \cdot \dot{\Delta}_c^{0.041} \ \text{[MPa]} \tag{12}$$

$$\text{Mix LF} \Rightarrow \sigma_f(\dot{\Delta}_c) = 6.47 \cdot \dot{\Delta}_c^{0.051} \ \text{[MPa]} \tag{13}$$

$$\text{Mix DF} \Rightarrow \sigma_f(\dot{\Delta}_c) = 5.77 \cdot \dot{\Delta}_c^{0.087} \ \text{[MPa]} \tag{14}$$

Subsequently, power laws (11) to (14) and the linear-elastic stress fields from the sharp-notched specimens were used to estimate the critical length values according to the simplified procedure shown in Fig. 2. The values of critical length L under quasi-static loading ($\dot{\Delta}_c \approx$

$0.02\ mm/s$) and critical length $L_D$ under dynamic loading ($\dot{\Delta}_c \approx 2.2\ mm/s$) were estimated for every mix design. These two values for $\dot{\Delta}_c$ were determined by averaging all the displacement rates applied (and measured) during testing under static and dynamic loading, respectively. Table 4 summarises the obtained values for L and $L_D$ and compares them with the size of the aggregates, $d_{agg}$, as well as with the average inter-aggregate distance, $d_s$.

Contrary to what one would expect based on the reasoning summarised at the beginning of the present section and based on the available knowledge, Tab. 4 makes it evident that, for the concrete mixes being investigated, the critical distance values were not linked in an evident, univocal way with either the aggregate size or the average inter-aggregate distance. Further, the results in the table show that the critical length was just marginally affected by the loading rate. Thus, the experimental evidence summarised in Tab. 4 suggests that, as far as concrete is concerned, the TCD critical distance may be linked to other relevant mesoscopic length scale parameters.

In order to try to identify possible alternative material meso-structural lengths, in what follows attention will be focused on the highly stressed regions - i.e., the areas in the vicinity of the notch tips, with the tensile stress in these regions being also responsible for the formation of the FPZ.

Initially, it is important to recall here that, as far as sharply notched beams loaded in bending are concerned, the level of stress multiaxility varies along the notch tip. The state of stress is biaxial on the two lateral surfaces (plane stress), with the degree of stress triaxility increasing as moving from the lateral surfaces themselves toward the mid-section of the beam [56]. If the thickness of the beam is large enough, then the triaxial state of stress at the centre of the beam is due to a fully developed plane strain condition. According to this well-known distribution of the stress along the notch tip line, the crack initiation process is then expected to take place mainly in a region close to the mid-section of the beam, i.e., in a region where the degree of triaxiliatiy of the stress (and the associated damage) reaches its maximum value.

Having reviewed this important stress analysis aspect, it can be recalled here also that, in general, engineering materials contain evenly spaced barriers [23]. These barriers play an

important role in defining the overall strength of materials since they can have a toughening effect by arresting the crack propagation process [54]. Under these circumstances, a crack can keep growing only if the loading is increased so that the crack itself is able to propagate by breaking through these toughening barriers. According to this reasoning, Taylor [54] argued that the TCD critical distance should be of the same order of magnitude as the average distance between adjacent barriers.

If attention is focussed specifically on unreinforced concrete, aggregates play the role of rigid inclusions that are way stronger than the cement paste - except for highly porous and weak aggregates [51]. Thus, both under static and low-dynamic loading, cracks are seen to initiate mainly in the cement paste or at the interface between the aggregates and cement paste itself [57].

According to the reasoning summarised above, one may argue that, in notched concrete components subjected to static/dynamic loading, the cracks initiate (at the notch tips) predominantly in those regions experiencing the largest degree of stress triaxiality. Subsequently, the cracks propagate until their growth is arrested (or, at least, slowed down) by the first aggregates that act as internal meso-structural barriers. This argument would then lead to the conclusion that the TCD critical distance is equal to distance $d_m$ (measured in the highly stressed region) between the notch tip and the first aggregate. For the sake of clarity, an example of a fracture surface with the suggested measurement for material length $d_m$ is presented in Fig. 8. According to Fig. 8, $d_m$ is measured at the mid section of the notched beam, i.e., at that section characterised by the larges degree of stress triaxiality. The average values for $d_m$ obtained according to this procedure are summarised in Tab. 4.

While this simple approach is certainly very appealing from a philosophical point of view, unfortunately, the direct comparison between lengths $d_m$, L and $L_D$ (see Tab. 4) makes it evident that the TCD critical distance is different from the average values being determined for $d_m$. It is the authors' opinion that this discrepancy between the TCD critical distance and $d_m$ can be ascribed to two key facts. First, the direct observation of the fracture surfaces revealed that, in some cases, there was a stone sitting at the mid-section of the specimen on

the notch tip (i.e., $d_m$=0 mm), with this situation making the interpretation and modelling of the fracture/toughening mechanisms in the highly stressed region more difficult. In particular, the fact that in some specimens $d_m$ was equal to zero did affect the average value obtained from the significant measurements, with this being accompanied by a relatively large value for the standard deviation (see Tab. 4). Second, given the nature of the fabrication process, concrete is highly non-uniform at a local/mesoscopic level. This is expected to result in crack initiations either occurring away from the mid-section (i.e., the section experiencing the largest level of stress triaxiality) or occurring simultaneously in multiple locations along the notch tip. These two aspects may explain why, as proven by the lengths listed in Tab. 4, it was observed a poor correlation between the TCD critical distance and $d_m$.

Taking as a starting point the reasoning summarised in the above paragraph, a subsequent attempt was then made to determine a relevant material length scale parameter, $d_c$, by averaging the distances between the first aggregates and the notch tip line across the specimen thickness. This was done by disregarding the presence of those aggregates directly sitting on the notch tip line. To better clarify this way of determining $d_c$, consider the schematic crack surface of a notched concrete specimen that is sketched in Fig. 9a. In this sketch, the shaded regions between the notch tip and the first aggregate particles indicate the material portions of interest, i.e., those regions used to estimate $d_c$. According to Fig. 9a, for any tested specimen, the area, $A_i$, and the width, $W_i$, of the regions of interest were determined using an image processing software [58], with this being done by analysing one of the two crack surfaces. Fig. 9b shows an example of the procedure that was followed to identify and measure the material areas of interest. Having determined $A_i$ and $W_i$ for a specific area, then the average length associated with the area under investigation was then calculated simply as $d_i=A_i/W_i$. Lastly, for any concrete mix design (i.e., either LD, DC, LF, or DF), the associated material length scale parameter $d_c$ was then calculated as follows:

$$d_c = \frac{1}{n}\sum_{i=1}^{n} d_i \tag{15}$$

where $n$ is the total number of the regions of interest identified and measured in all the notched specimens being tested (i.e., considering the results generated under both static and dynamic loading). This simple procedure returned the following values for material length $d_c$ (see also Tab. 4): 5.3 mm for LC, 4.7 mm for DC, 4.7 mm for LF, and 4.3 mm for DF. The results reported in Tab. 4 show that, given the different concrete mixes, the calculated values for $d_c$ were not only characterised by a low value of the associated standard deviation, but also close to the corresponding values of the TCD critical distances calculated under quasi-static (L) and under dynamic loading ($L_D$). It is important to point out here that the limited variation in the $d_c$ lengths that were obtained for the different mixes is clearly due to the strategy that was followed to determine the $d_c$ values themselves. In particular, the estimation of $d_c$ involved ignoring those portions of material where the aggregates where directly sitting on the notch tip line, with this affecting the lengths determined according to Eq. (15).

As far as unreinforced concrete is concerned, the considerations reported above together with the results summarised in Tab. 4 seem to strongly support the idea that the TCD critical distance is directly linked with the average distance between the potential superficial crack initiation points and the first aggregates which act as inherent meso-structural barriers.

According to this physical model, the TCD critical distance was then taken constant and equal to the average value of $d_c$ measured from all the notched specimens being tested, that is:

$$\mathrm{L}\left(\dot{\Delta}_c\right) = 4.8\ mm \tag{16}$$

This value for $\mathrm{L}\left(\dot{\Delta}\right)$ was then used along with the TCD as reviewed in Section 2 by assuming that the required critical distance was known *a priori* from the material morphology (and, therefore, not determined experimentally according to the procedure summarised in Fig. 2). The accuracy of the TCD when applied according to this alternative strategy to determine $\mathrm{L}\left(\dot{\Delta}\right)$ was assessed by calculating the error via the following standard relationship:

$$Error = \frac{\sigma_{eff}(\dot{\Delta}_c) - \sigma_f(\dot{\Delta}_c)}{\sigma_f(\dot{\Delta}_c)} [\%] \quad (17)$$

The overall accuracy of the TCD applied in the form of the PM and LM in estimating the static and dynamic strength of notched concrete is summarised in Fig. 10. According to the error vs. displacement rate diagram reported in Fig. 10, the estimates obtained by taking $L(\dot{\Delta}_c)$ invariably equal to 4.8 mm were seen to fall mainly within an error band of ±20%. This level of accuracy is certainly satisfactory because, as argued by David Taylor [23], it is impossible to distinguish between an error of 0% and 20% due to inherent experimental and numerical errors.

## 5 Conclusions

As far as unreinforced concrete is concerned, a systematic experimental/theoretical investigation was carried out in order to establish rigorous links between the TCD critical distance and the material mesoscopic structural features. To this end, a number of experiments were run by using special concrete mixes that were designed to obtain controlled material mesoscopic morphologies. This suggests that more work needs to be done in order to further validate the outcomes from the present theoretical/experimental investigation with concrete materials manufactured using different mixes and different manufacturing procedures. Having highlighted this important aspect, the key conclusions from this study are summarized in what follows.

- There exist a direct inter-correlation between mesoscopic morphology of concrete and TCD critical distance.
- The TCD critical distance appears not to be directly linked with the average aggregate size or the average inter-aggregate distance.
- The TCD critical length is seen to approach the average distance between the notch tip line and the first aggregates, with these aggregates acting as barriers slowing down/affecting the crack propagation process.

- The mechanical behaviour/properties of concrete are size-dependent, accordingly, more work needs to be done in order to understand possible links between size effect, TCD critical distance and concrete material mesoscopic structural features.

**ACKNOWLEDGMENT**

Support for this research work from the Engineering and Physical Sciences Research Council (EPSRC, UK) through the award of grant EP/S019650/1 is gratefully acknowledged. Nasser A. Alanazi is grateful to the University of Hail, Saudi Arabia, for sponsoring his PhD studentship.

## References

[1] Anderson T. Fracture mechanics: fundamentals and applications. 3rd Edition, CRC Press, USA, 2005.

[2] Bažant ZP. Mechanics of fracture and progressive cracking in concrete structures. In: Sih G.C., Di Tommaso A. (eds), Fracture mechanics of concrete: Structural application and numerical calculation. Engineering Application of Fracture Mechanics, Vol 4. Springer, Dordrecht, 1985 - https://doi.org/10.1007/978-94-009-6152-4_1

[3] Bažant ZP. Concrete fracture models: testing and practice. Eng Fract Mech 2002;69:165–205.

[4] Cedolin L, Cusatis G. Identification of concrete fracture parameters through size effect experiments. Cem Concr Compos 2008;30:788–797.

[5] Hu X, Wittmann FH. Experimental method to determine extension of fracture-process zone. J Mater Civ Eng 1990;2:15–23.

[6] Nemati KM. Fracture analysis of concrete using scanning electron microscopy. Scanning 1997;19:426–430.

[7] Mindess S, Diamond S. A device for direct observation of cracking of cement paste or mortar under compressive loading within a scanning electron microscope. Cem Concr Res 1982;12:569–576.

[8] Mindess S, Diamond S. A preliminary SEM study of crack propagation in mortar. Cem Concr Res 1980;10:509–519.

[9] Slate FO, Olsefski S. X-Rays for Study of Internal Structure and Microcracking of Concrete. ACI J Proc 1963;60:575–588 - https://doi.org/10.14359/7869

[10] Robinson SR. Methods of determining the formation and propagation of microcracking in concrete. In: Brooks A.E. and Newman K. (eds), The Structure of Concrete, Cement and Concrete Association, London, UK, 1968, p. 131–145.

[11] Saliba J, Loukili A, Regoin J-P, Grégoire D, Verdon L, Pijaudier-Cabot G. Experimental analysis of crack evolution in concrete by the acoustic emission technique. Frat Integrita Strutt 34;2015:300-308.

[12] Saliba J, Matallah M, Loukili A, Regoin J-P, Grégoire D, Verdon L, Pijaudier-Cabot G.

Experimental and numerical analysis of crack evolution in concrete through acoustic emission technique and mesoscale modelling. Eng Fract Mech 167;2016:123–137.

[13] Maji A, Shah SP. Process zone and acoustic-emission measurements in concrete. Exp Mech 28;1988:27–33.

[14] Maji AK, Ouyang C, Shah SP. Fracture mechanisms of quasi-brittle materials based on acoustic emission. J Mater Res 5;1990:206–217.

[15] Sakata Y, Ohtsu M. Crack evaluation in concrete members based on ultrasonic spectroscopy. Materials Journal 92;1995:686–698.

[16] Otsuka K, Date H. Fracture process zone in concrete tension specimen. Eng Fract Mech 65;2000:111–131.

[17] Mihashi H, Nomura N, Niiseki S. Influence of aggregate size on fracture process zone of concrete detected with three dimensional acoustic emission technique. Cem Concr Res 21;1991:737–744.

[18] Ceriolo L, Di Tommaso A. Fracture mechanics of brittle materials: a historical point of view. In: 2nd International PhD Symposium in Civil Engineering. Budapest, Hungary, 1998.

[19] Bažant ZP. Mechanics of fracture and progressive cracking in concrete structures. In: Sih C. and Di Tommaso A. (eds), Fracture mechanics of concrete: Structural application and numerical calculation, Kluver Academic Publishers, Dordrechtt, the Netherlands, 1985.

[20] Hillerborg A, Modéer M, Petersson PE. Analysis of crack formation and crack growth in concrete by means of fracture mechanics and finite elements. Cem Concr Res 1976;6:773–781.

[21] Bažant ZP, Oh BH. Crack band theory for fracture of concrete. Mat Constr 1983;16:155–177.

[22] Murthy ARC, Palani GS, Iyer NR. State-of-the-art review on fracture analysis of concrete structural components, Sadhana 2009;34:345–367.

[23] Taylor D. The Theory of Critical Distances: a New Perspective in fracture mechanics, Elsevier, Oxford, UK, 2007 - https://doi.org/10.1016/B978-0-08-044478-9.X5000-5.

[24] Shah SP, Swartz SE, Ouyang C. Fracture mechanics of concrete: applications of fracture mechanics to concrete, rock and other quasi-brittle materials. John Wiley & Sons, New York, USA, 1995 - ISBN: 0-471-30311-9

[25] Karihaloo BL. Fracture mechanics & structural concrete. Longman Scientific & Technical, 1995 - ISBN: 9780582215825.

[26] Pelekis I, Susmel L. The Theory of Critical Distances to assess failure strength of notched plain concrete under static and dynamic loading. Eng Fail Anal 2017;82:378–389.

[27] Yin T, Tyas A, Plekhov O, Terekhina A, Susmel L. A novel reformulation of the Theory of Critical Distances to design notched metals against dynamic loading. Mater Des 2015;69:197–212 - https://doi.org/https://doi.org/10.1016/j.matdes.2014.12.026.

[28] Susmel L. Multiaxial notch fatigue: from nominal to local stress–strain quantities, Woodhead & CRC, Cambridge, UK, 2009.

[29] Taylor D. Predicting the fracture strength of ceramic materials using the theory of critical distances. Eng Fract Mech 2004;71:2407–2416.

[30] Taylor D, Merlo M, Pegley R, Cavatorta MP. The effect of stress concentrations on the fracture strength of polymethylmethacrylate. Mater Sci Eng A 2004;382:288–294.

[31] Whitney JM, Nuismer RJ. Stress fracture criteria for laminated composites containing stress concentrations, J Compos Mater 1974;8:253–265.

[32] Jadallah O, Bagni C, Askes H, Susmel L. Microstructural length scale parameters to model the high-cycle fatigue behaviour of notched plain concrete. Int J Fatigue 2016;82:708–720 - https://doi.org/10.1016/j.ijfatigue.2015.09.029.

[33] Askes H, Aifantis EC. Gradient elasticity in statics and dynamics: an overview of formulations, length scale identification procedures, finite element implementations and new results. Int J Solids Struct 2011;48:1962–1990.

[34] Gitman IM, Askes H, Aifantis EC. The representative volume size in static and dynamic micro-macro transitions. Int J Fract 2005;135:L3--L9.

[35] Susmel L, Askes H, Bennett T, Taylor D. Theory of critical distances versus gradient mechanics in modelling the transition from the short to long crack regime at the fatigue limit. Fatigue Fract Eng Mater Struct 2013;36:861–869.

[36] Shah SP. Determination of fracture parameters ($K^s_{IC}$ and CTODc) of plain concrete using three-point bend tests. Mater Struct 1990;23:457–460.

[37] Malvar LJ, Crawford JE. Dynamic Increase Factors, Twenty-Eighth DDESB Seminar, Orlando, Florida, USA, August 1998.

[38] Bischoff PH, Perry SH. Compressive behaviour of concrete at high strain rates. Mater Struct 1991;24:425–450 - https://doi.org/10.1007/BF02472016.

[39] Chen X, Wu S, Zhou J. Experimental study on dynamic tensile strength of cement mortar using split Hopkinson pressure bar technique. J Mater Civ Eng 2014;26(6):04014005.

[40] Adhikary SD, Li B, Fujikake K. State-of-the-art review on low-velocity impact response of reinforced concrete beams. Mag Concr Res 2016;68:701–723.

[41] Lambert DE, Allen Ross C. Strain rate effects on dynamic fracture and strength. Int J Impact Eng 2000;24:985–998 - https://doi.org/https://doi.org/10.1016/S0734-743X(00)00027-0.

[42] John R, Shah SP. Mixed-mode fracture of concrete subjected to impact loading. J Struct Eng 1990;116:585–602.

[43] Peterson RE. Notch sensitivity. In: Sines G., Waisman J.L. (eds.), Metal fatigue, McGraw Hill, New York, 1959, pp. 293-306.

[44] H. Neuber, Theorie der technischen Formzahl. Forschung a d Geb d Ingenieurwes 1936;7:271–274.

[45] Neuber H. Theory of notch stresses: principles for exact calculation of strength with reference to structural form and material (2nd Ed.), Springer Verlag, Berlin, 1958.

[46] Taylor D, Wang G. Validation of some methods of notch fatigue analysis. Fatigue Fract Eng Mater Struct 2000;23:387–394 - https://doi.org/10.1046/j.1460-2695.2000.00302.x.

[47] Taylor D. Geometrical effects in fatigue: a unifying theoretical model. Int J Fatigue 1999;21:413–420 - https://doi.org/https://doi.org/10.1016/S0142-1123(99)00007-9.

[48] Bellett D, Taylor D, Marco S, Mazzeo E, Guillois J, Pircher T. The fatigue behaviour of three-dimensional stress concentrations. Int J Fatigue 2005;27:207–221.

[49] Susmel L, Taylor D. The Theory of Critical Distances as an alternative experimental strategy for the determination of $K_{Ic}$ and $\Delta K_{th}$. Eng Fract Mech 2010;77:1492–1501. https://doi.org/https://doi.org/10.1016/j.engfracmech.2010.04.016.

[50] Di Tommaso A. Evaluation of concrete fracture. In: Carpinteri A., Ingraffea A.R. (eds), Fracture mechanics of concrete: Material characterization and testing. Engineering Application of Fracture Mechanics, vol 3. Springer, Dordrecht, 1984 - https://doi.org/10.1007/978-94-009-6149-4_2

[51] Mehta PK, Monteiro PJM. Concrete: microstructure, properties, and materials. 3rd edit, McGraw-Hill, New York, USA, 2014.

[52] Alanazi N, Susmel L. Estimating static/dynamic strength of notched unreinforced concrete under mixed-mode I/II loading. Eng Fract Mech 2020;240:107329 - https://doi.org/https://doi.org/10.1016/j.engfracmech.2020.107329.

[53] Susmel L, Taylor D. A novel formulation of the theory of critical distances to estimate lifetime of notched components in the medium-cycle fatigue regime. Fatigue Fract Eng Mater Struct 2007;30:567–581.

[54] Taylor D. The Theory of Critical Distances: A link to micromechanisms. Theor Appl Fract Mech 2017;90:228–233 - https://doi.org/https://doi.org/10.1016/j.tafmec.2017.05.018.

[55] Shafigh P, Bin Mahmud H, Jumaat MZ, Zargar M. Agricultural wastes as aggregate in concrete mixtures – A review. Constr Build Mater 2014;53:110–117 - https://doi.org/https://doi.org/10.1016/j.conbuildmat.2013.11.074.

[56] Meneghetti G, Susmel L, Tovo R. High-cycle fatigue crack paths in specimens having different stress concentration features. Eng Fail Anal 2007;14:656–672.

[57] Gatuingt F, Snozzi L, Molinari J-F. Numerical determination of the tensile response and the dissipated fracture energy of concrete: role of the mesostructure and influence of the loading rate. Int J Numer Anal Methods Geomech 2013;37:3112–3130.

[58] Schneider C, Rasband W, Eliceiri K. NIH Image to ImageJ: 25 years of image analysis. Nat Methods 2012;9:671–675 - https://doi.org/10.1038/nmeth.2089

**List of Captions**

| | Materials by weight (kg/m$^3$) | | | | | |
|---|---|---|---|---|---|---|
| Mix ID | Cement | Aggregate | Sand | Water | Superplasticizer | Aggregate size[(a)], $d_{agg}$, (mm) |
| LC | 450.0 | 687.0 | 964.0 | 198.0 | 2.0 | 10.5 |
| DC | 450.0 | 964.0 | 687.0 | 198.0 | 13.3 | 10.5 |
| LF | 450.0 | 687.0 | 964.0 | 198.0 | 2.0 | 5.5 |
| DF | 450.0 | 1075.0 | 576.0 | 198.0 | 13.3 | 5.5 |

[(a)] Single-size aggregates.

**Table 1.** Details of concrete mix proportions and aggregate sizes used in this study.

| Mix ID | Loading Method | Specimen Code | Width (mm) | Thickness (mm) | Time to failure (s) | Displacement rate[a] (mm/s) | Failure Force (kN) |
|---|---|---|---|---|---|---|---|
| LC | Static | LC1-1 | 50.03 | 75.23 | 4.500 | 0.0177 | 3.088 |
| | | LC1-2 | 50.13 | 74.86 | 4.620 | 0.0162 | 3.003 |
| | | LC1-3 | 50.47 | 75.95 | 7.570 | 0.0123 | 2.895 |
| | Dynamic | LC2-1 | 50.45 | 75.08 | 0.039 | 2.4676 | 3.185 |
| | | LC2-2 | 50.01 | 75.32 | 0.038 | 1.7332 | 3.580 |
| | | LC2-3 | 50.47 | 74.75 | 0.040 | 2.5566 | 3.607 |
| DC | Static | DC1-1 | 50.12 | 77.03 | 4.930 | 0.0155 | 2.391 |
| | | DC1-2 | 50.27 | 75.80 | 5.170 | 0.0146 | 2.888 |
| | | DC1-3 | 50.28 | 75.55 | 3.150 | 0.0239 | 2.859 |
| | Dynamic | DC2-1 | 50.06 | 77.28 | 0.025 | 3.5397 | 3.284 |
| | | DC2-2 | 50.36 | 77.88 | 0.050 | 1.6236 | 3.487 |
| | | DC2-3 | 50.11 | 77.52 | 0.044 | 2.1319 | 3.315 |
| LF | Static | LF1-1 | 50.10 | 77.97 | 5.550 | 0.0166 | 3.245 |
| | | LF1-2 | 50.30 | 77.04 | 6.750 | 0.0164 | 3.139 |
| | | LF1-3 | 50.14 | 77.92 | 4.660 | 0.0210 | 2.774 |
| | Dynamic | LF2-1 | 50.13 | 75.64 | 0.045 | 2.3162 | 3.896 |
| | | LF2-2 | 50.26 | 74.54 | 0.045 | 1.9454 | 3.795 |
| | | LF2-3 | 50.24 | 74.48 | 0.041 | 2.8716 | 3.674 |
| DF | Static | DF1-1 | 50.14 | 75.51 | 3.410 | 0.0119 | 2.146 |
| | | DF1-2 | 50.24 | 75.46 | 6.230 | 0.0097 | 2.209 |
| | Dynamic | DF2-1 | 50.16 | 75.66 | 0.043 | 2.4052 | 3.686 |
| | | DF2-2 | 50.37 | 75.12 | 0.055 | 0.7504 | 3.283 |
| | | DF2-3 | 49.92 | 76.32 | 0.032 | 2.4632 | 3.268 |

[a] Calculated from measuring vertical displacement on the bottom and mid-span of the specimens using DIC.

**Table 2**. Summary of the results obtained from testing plain specimens under 3PB.

| Mix ID | Loading Method | Specimen Code | Notch depth (mm) | Width (mm) | Thickness (mm) | Time to failure (s) | Displacement rate[(a)] (mm/s) | Failure Force (kN) |
|---|---|---|---|---|---|---|---|---|
| LC | Static | LC1-S1 | 24.82 | 75.36 | 75.86 | 10.130 | 0.0076 | 2.437 |
| | | LC1-S2 | 25.05 | 75.35 | 76.20 | 4.300 | 0.0139 | 2.847 |
| | | LC1-S3 | 25.19 | 75.76 | 75.75 | 4.480 | 0.0116 | 2.932 |
| | Dynamic | LC2-S1 | 24.87 | 75.36 | 74.99 | 0.034 | 1.9948 | 3.150 |
| | | LC2-S2 | 25.01 | 75.33 | 74.98 | 0.045 | 1.0265 | 3.577 |
| | | LC2-S3 | 24.90 | 75.08 | 75.69 | 0.049 | 1.4633 | 3.361 |
| DC | Static | DC1-S1 | 24.67 | 74.95 | 76.00 | 5.860 | 0.0146 | 2.982 |
| | | DC1-S2 | 25.19 | 75.69 | 76.24 | 4.480 | 0.0129 | 2.645 |
| | | DC1-S3 | 24.92 | 75.16 | 75.55 | 5.260 | 0.0091 | 2.708 |
| | Dynamic | DC2-S1 | 25.22 | 75.24 | 77.06 | 0.049 | 2.0377 | 2.808 |
| | | DC2-S2 | 25.07 | 75.37 | 76.86 | 0.041 | 1.5152 | 2.825 |
| | | DC2-S3 | 24.99 | 75.30 | 76.94 | 0.039 | 2.4276 | 2.881 |
| LF | Static | LF1-S1 | 24.72 | 75.18 | 76.46 | 6.160 | 0.0174 | 2.478 |
| | | LF1-S2 | 25.19 | 75.35 | 77.35 | 5.010 | 0.0152 | 3.009 |
| | | LF1-S3 | 24.91 | 75.20 | 77.25 | 4.940 | 0.0153 | 2.964 |
| | Dynamic | LF2-S1 | 34.17 | 74.98 | 74.74 | 0.031 | 1.1914 | 2.852 |
| | | LF2-S2 | 24.82 | 75.25 | 76.56 | 0.044 | 3.9115 | 3.014 |
| | | LF2-S3 | 25.31 | 75.39 | 75.96 | 0.036 | 2.0348 | 3.519 |
| DF | Static | DF1-S1 | 24.79 | 75.17 | 74.85 | 3.620 | 0.0120 | 2.603 |
| | | DF1-S2 | 24.94 | 75.30 | 75.13 | 3.060 | 0.0216 | 2.432 |
| | | DF1-S3 | 25.01 | 75.28 | 75.48 | 7.770 | 0.0180 | 2.569 |
| | Dynamic | DF2-S1 | 34.10 | | 75.39 | 0.036 | 2.4419 | 3.139 |
| | | DF2-S2 | 24.89 | 75.53 | 75.85 | 0.039 | 2.4907 | 3.560 |
| | | DF2-S3 | 24.77 | 75.27 | 74.91 | 0.0679 | 0.9100 | 3.467 |

[(a)] Calculated from measuring vertical displacement at the notch tip

**Table 3**. Summary of the results obtained from testing notched specimens under 3PB.

| Mix ID | L (mm) | $L_D$ (mm) | $d_{agg}$ (mm) | $d_s$ (mm) | $d_m$ (mm) | $d_c$ (mm) |
|---|---|---|---|---|---|---|
| LC | 4.7 | 5.3 | 10.5 | 4.8 | 2.1 | 5.3 |
| DC | 5.8 | 4.4 | 10.5 | 2.8 | 2.5 | 4.7 |
| LF | 5.0 | 4.0 | 5.5 | 3.3 | 3.3 | 4.7 |
| DF | 6.3 | 5.3 | 5.5 | 1.9 | 3.1 | 4.3 |
| *Average* | *5.5* | *4.8* | - | - | *2.8* | *4.8* |
| *Standard Deviation* | *0.63* | *0.57* | - | - | *0.48* | *0.36* |

**Table 4.** Comparing the empirical values of the TCD critical distance with different meso-structural lengths characterising the concrete mixes being tested.

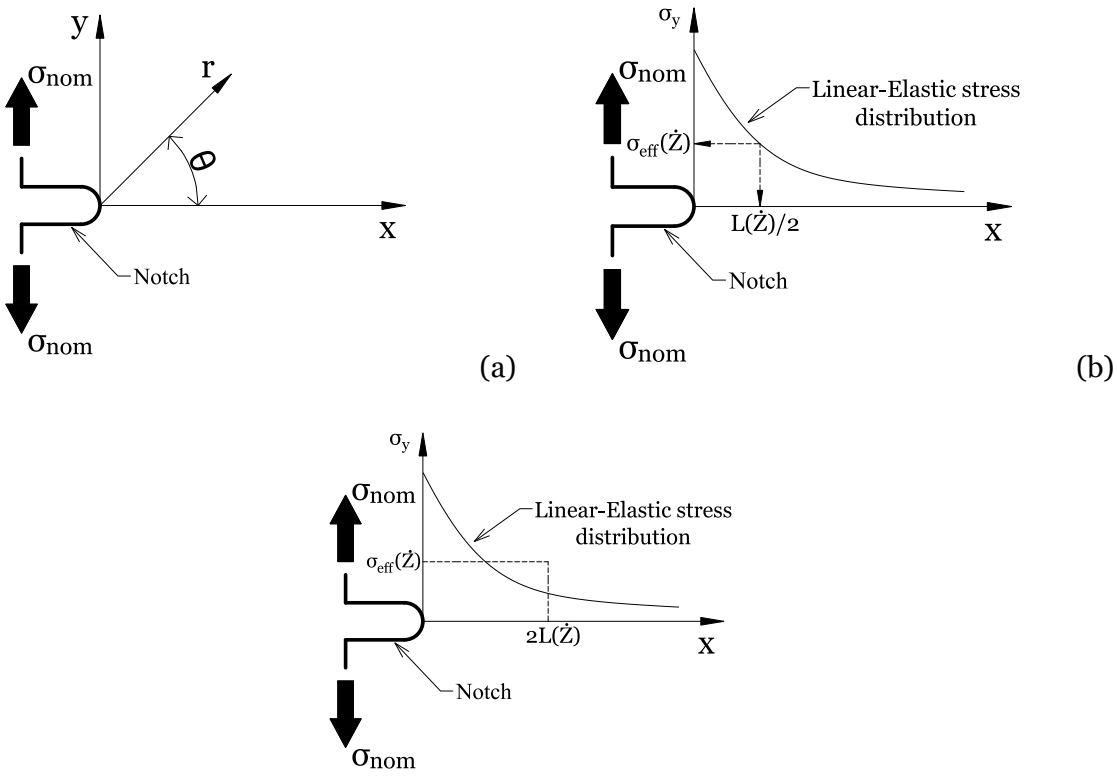


**Figure 1.** Local system of coordinates (a); calculation of the dynamic effective stress according to the PM (b) and LM (C).

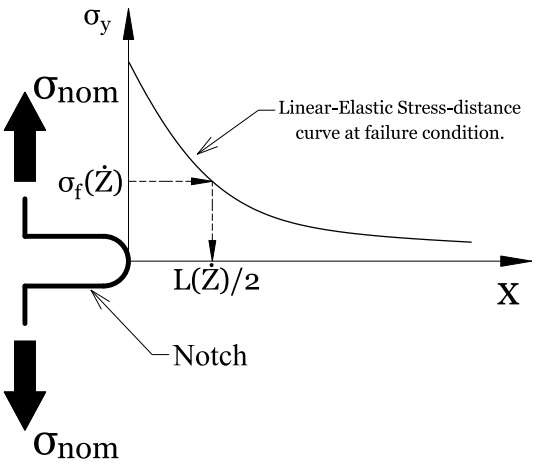


**Figure 2.** Alternative procedures to estimate $\mathbf{L}(\dot{\mathbf{Z}})$ according to the PM.

(a) $d_g$ ≈10.50 mm (b) $d_g$ ≈5.50 mm

**Figure 3.** The used single-size aggregate particles.

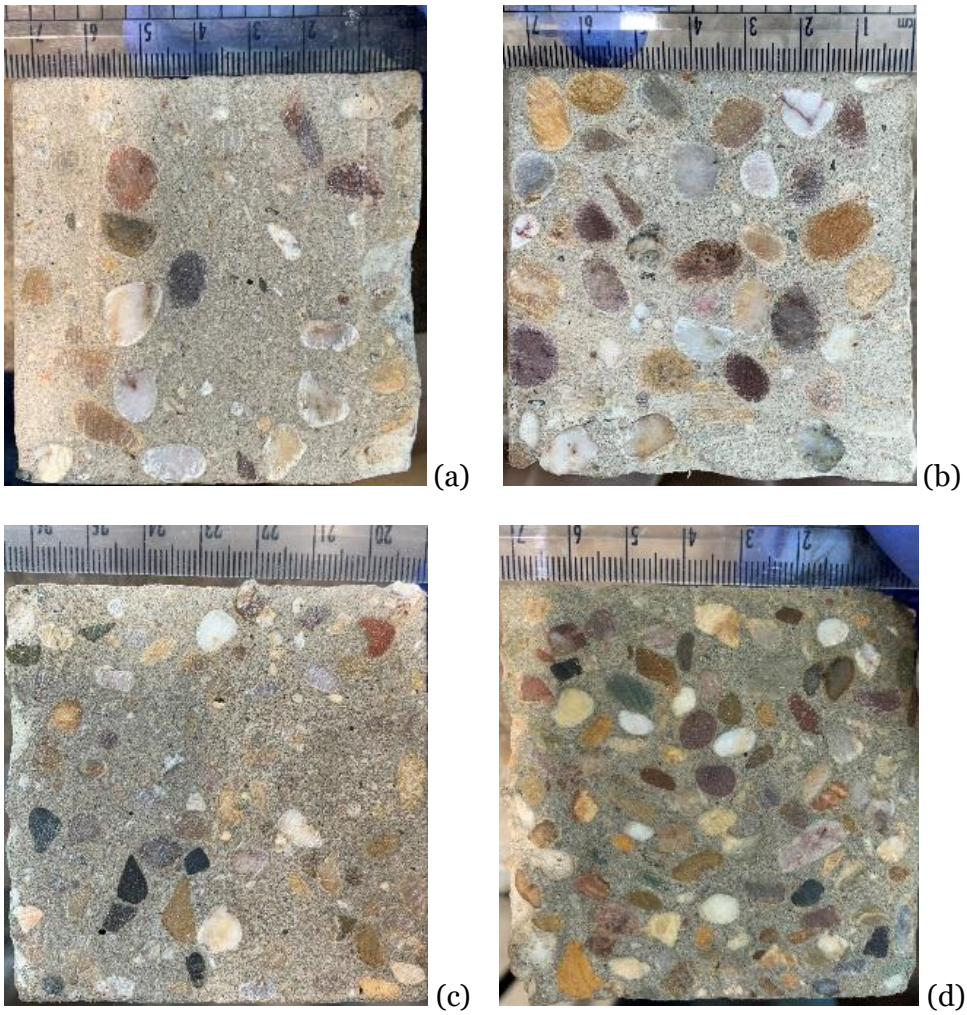


**Figure 4.** Example pictures of cut cross-sections taken to quantify the average spacing between aggregates of LC (a), DC (b), LF (c), and DF (d) concrete mixes.

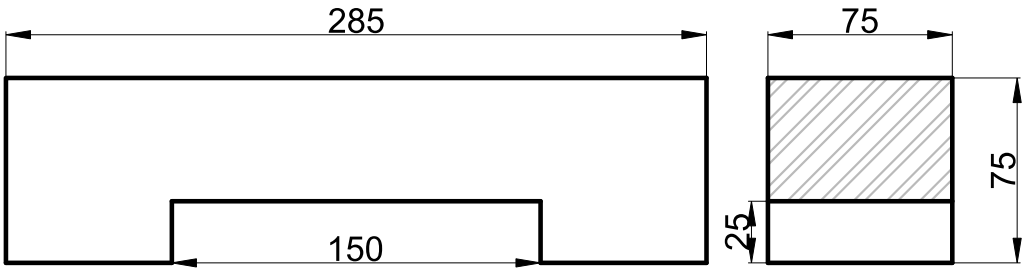


(a)

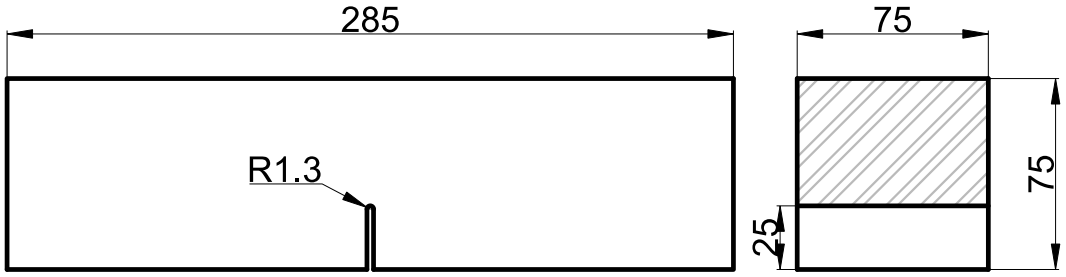


(b)

**Figure 5.** Geometries of the un-notched (a) and notched (b) specimens.

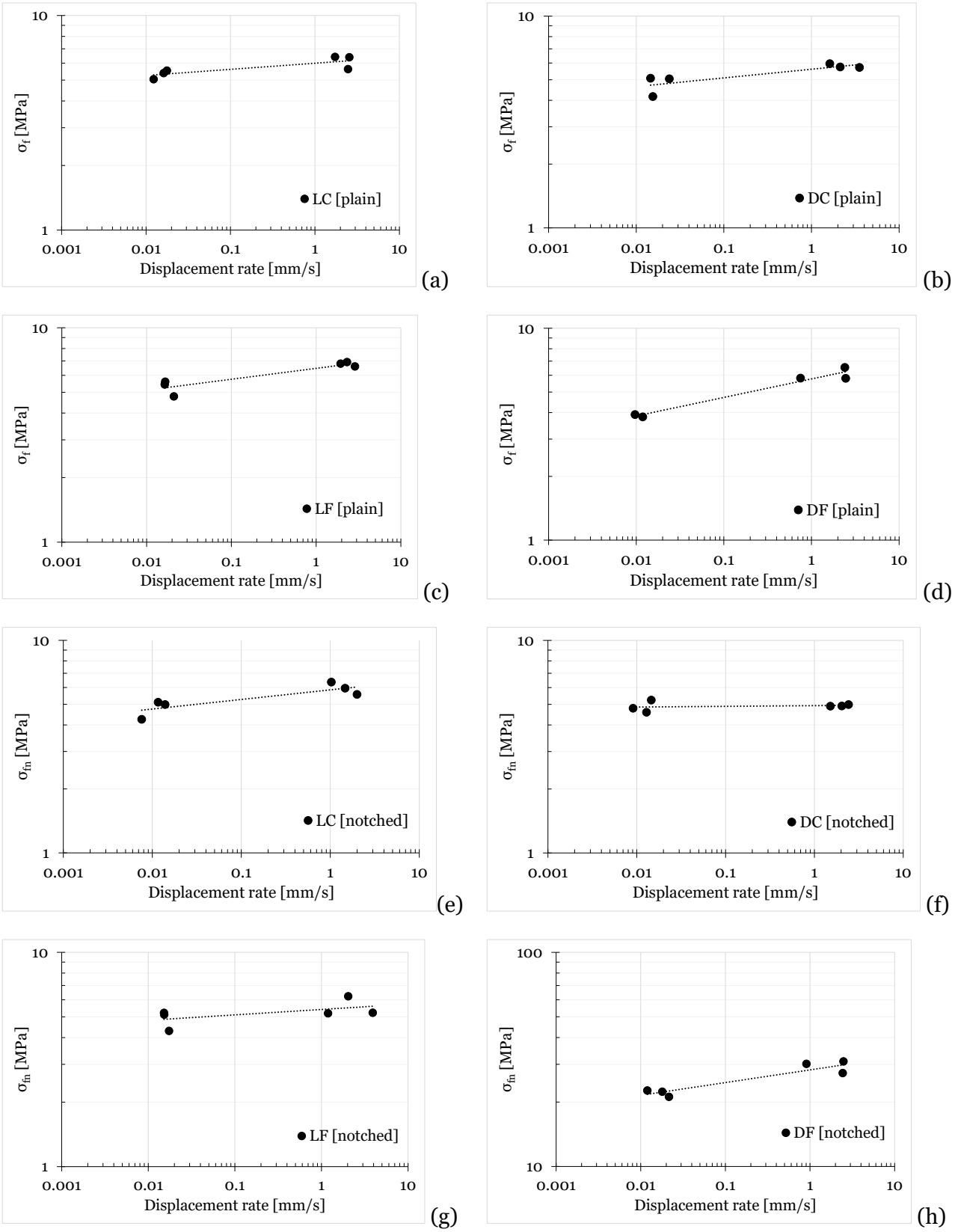


**Figure 6.** Experimental results obtained from testing un-notched (a-d) and notched (e-h) specimens prepared from different concrete mix designs.

| Mix ID | Static Loading | Dynamic Loading |
|---|---|---|
| LC |  LC1-S3 |  LC2-S1 |
| DC |  DC1-S3 |  DC2-S2 |
| LF |  LF1-S3 |  LF2-S2 |
| DF |  DF1-S1 |  DF2-S2 |

**Figure 7.** Examples of fracture surfaces generated by testing notched specimens under static (left) and dynamic (right) loading.

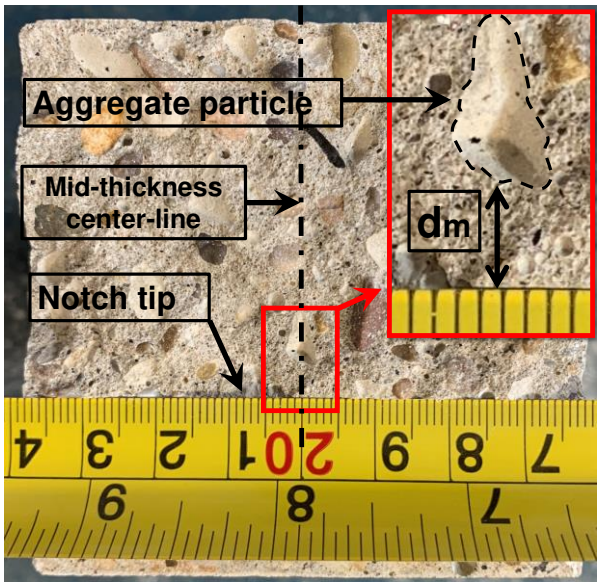


**Figure 8.** Example of measuring $d_m$ at the mid-thickness for LF1-S1.

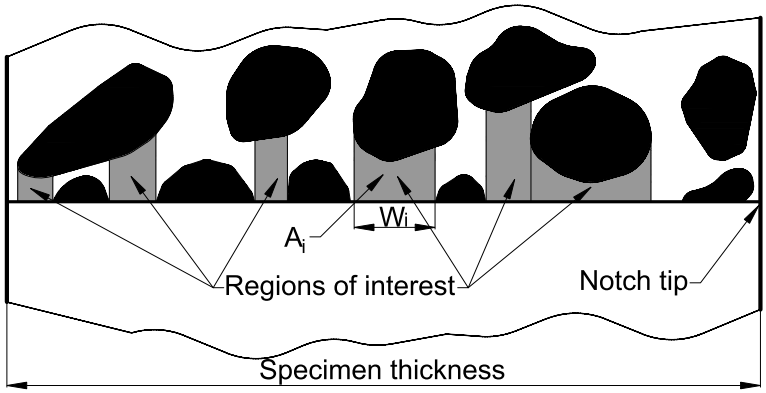


**(a)**

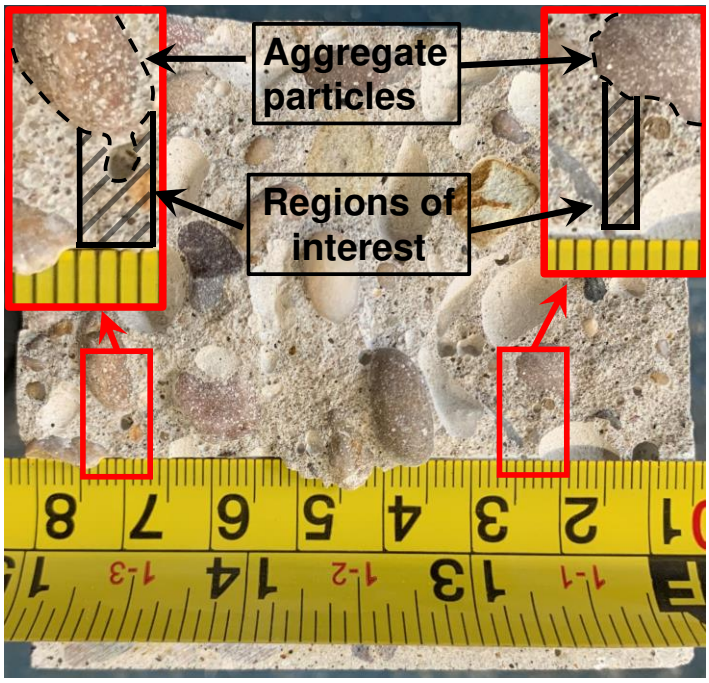


**(b)**

**Figure 9.** Schematic illustration of identifying the regions of interest between the notch tip and first aggregate barrier, $A_i$, and $W_i$ (a) and example of locating the regions of interest on the fracture surface of specimen DC1-S2 (b).

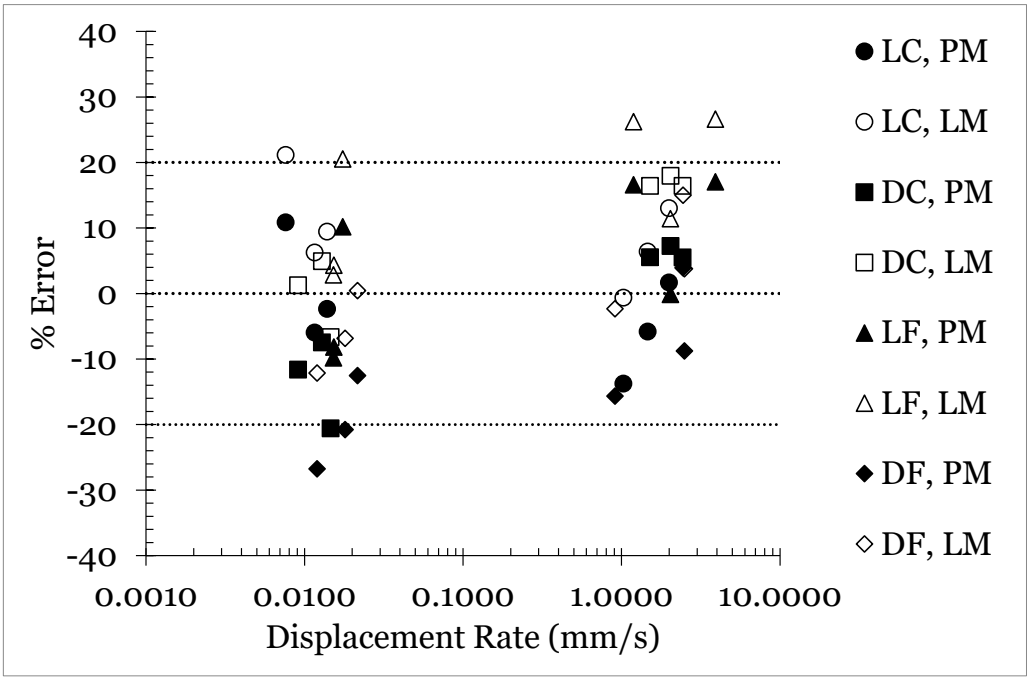


**Figure 10.** Accuracy of the PM and LM in estimating the static and dynamic strength of notched concrete based on the proposed physical measurements of L.